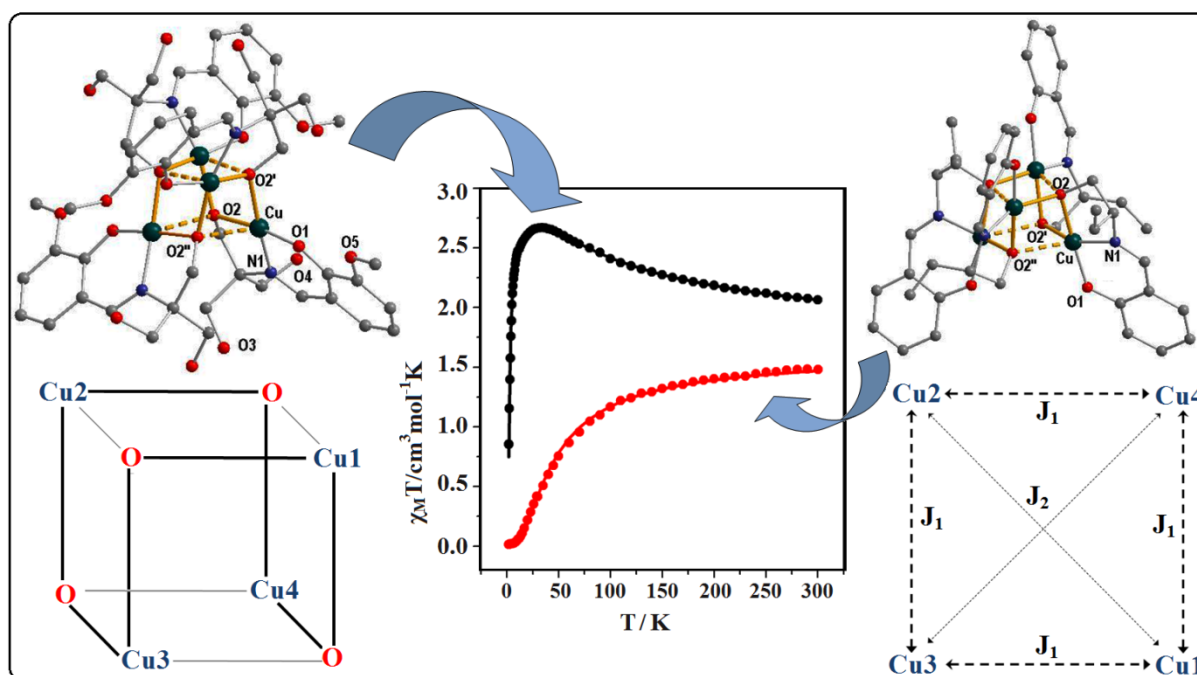


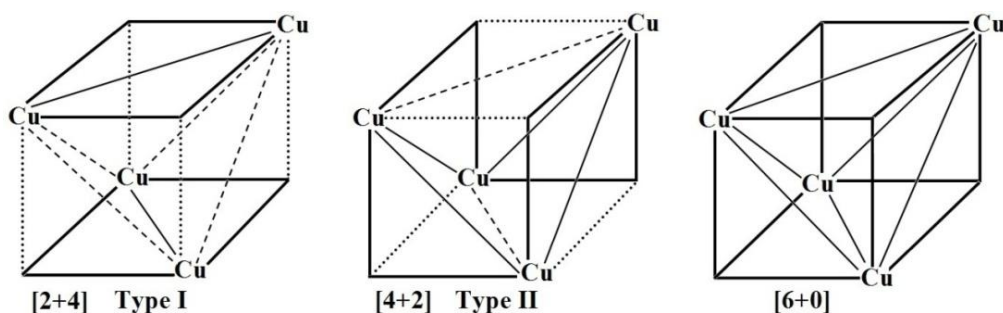
## Chapter III

### *Structural and Magnetic Characterization of Two Tetranuclear Cu(II) Complexes with Closed-Cubane-Like Core Framework*



### 3.1. Introduction

Polynuclear 3d-metal coordination compounds have attracted continuous attention in the recent decades due to their interesting structure and molecular properties.<sup>[3.1]</sup> Among the high nuclear complexes,  $M_4X_4$  (where  $M=Cu, Ni, Co, Fe, Mn$ ;  $X= O, S$ ) have been broadly investigated for their relevance in the field of magnetism,<sup>[3.2]</sup> catalysis<sup>[3.3]</sup> and bio-inorganic chemistry.<sup>[3.4]</sup> In particular  $Cu_4O_4$  alkoxo, hydroxo and phenoxo bridged cubane like complexes have been widely studied adopting experimental and theoretical approach for exploring their magneto-structural correlation.<sup>[3.5]</sup> Based on the arrangement and connectivity of the copper and oxygen atom in the tetranuclear  $Cu_4O_4$  core, the cubane geometries may be of various types e.g; regular cubane,<sup>[3.6]</sup> single-open cubane,<sup>[3.7]</sup> double-open cubane<sup>[3.8]</sup> and face sharing dicubane.<sup>[3.9]</sup> Depending on the distribution of Cu-O bond distances in the cube, Mergehenn and Haase classified cubane of type I and type II.<sup>[3.10]</sup>  $Cu_4O_4$  cubane complexes having four long Cu-O distances between two dinuclear subunits are designated as type I, whereas if the long Cu-O distances are within each dinuclear subunit, cubanes are classified as type II.<sup>[3.11,3.18]</sup> On the other hand, taking into account the  $Cu\cdots Cu$  distances within the  $Cu_4O_4$  cubane unit, Alvarez *et al.* described<sup>[3.12]</sup> three types (Scheme 3.1) the compounds: (i) (2+4) having two short and four long  $Cu\cdots Cu$  distances, which is equivalent to type I (defined above); (ii) (4+2) with four short and two long  $Cu\cdots Cu$  distances, an equivalent description to type II and (iii) (6+0), where all six  $Cu\cdots Cu$  bonds have comparable distances.



Scheme 3.1. Classification of  $Cu_4O_4$  core (schematic figure) according to the  $Cu\cdots Cu$  distances. Short  $Cu\cdots Cu$  distances, long  $Cu\cdots Cu$  distances, short  $Cu\cdots O$  bond lengths and long  $Cu\cdots O$  bond lengths are shown in solid lines, dashed lines, bold lines and square dots respectively.

Polydentate Schiff base ligands possessing alkoxo, hydroxo and phenoxo donor centers are potential ligand for the synthesis of multinuclear copper complexes. As an extension in the synthesis of cubane copper compounds we have used two Schiff bases namely (E)-2-((1-hydroxybutan-2-ylimino)methyl) phenol ( $H_2L^1$ ) and 2-((2-hydroxy-3-methoxybenzylidene)amino)-2-hydroxymethylpropane-1,3-diol ( $H_4L^2$ ), which have potentiality to coordinate metal ions with alkoxo, hydroxo and phenoxo donor centres. In the present contribution we report the synthesis, the crystal structure and magnetic properties of two copper complexes  $[Cu_4(L^1)_4] \cdot 3(H_2O)$  (**1**) and  $[Cu_4(H_2L^2)_4(H_2O)_4]$  (**2**), both comprising a closed cubane like core structure.

## 3.2. Experimental

### 3.2.1. Materials and Physical Measurements

High purity 2-amino-1-butanol was purchased from Alfa-Aesar. All other chemicals were commercially available reagent grade and used as received. Solvents used for spectroscopic studies were purified and dried by standard procedures before use.<sup>[3,13]</sup>

Elemental analyses (carbon, hydrogen and nitrogen) were performed using a Perkin–Elmer 240C elemental analyzer. Electronic absorption spectra were obtained with a Shimadzu UV-1601 UV–Vis spectrophotometer at room temperature. Quartz cuvettes with a 1 cm path length and a 3 cm<sup>3</sup> volume were used for all measurements. IR spectra were recorded as KBr pellets on a Bruker Vector 22 FT IR spectrophotometer operating from 400 to 4000 cm<sup>-1</sup>. Emission spectra were recorded on a Hitachi F-7000 spectrofluorimeter. Room temperature (300 K) spectra were obtained in methanol solution using a quartz cell of 1 cm path length. <sup>1</sup>H and <sup>13</sup>C NMR spectra were recorded on a Varian 400 MHz instrument.

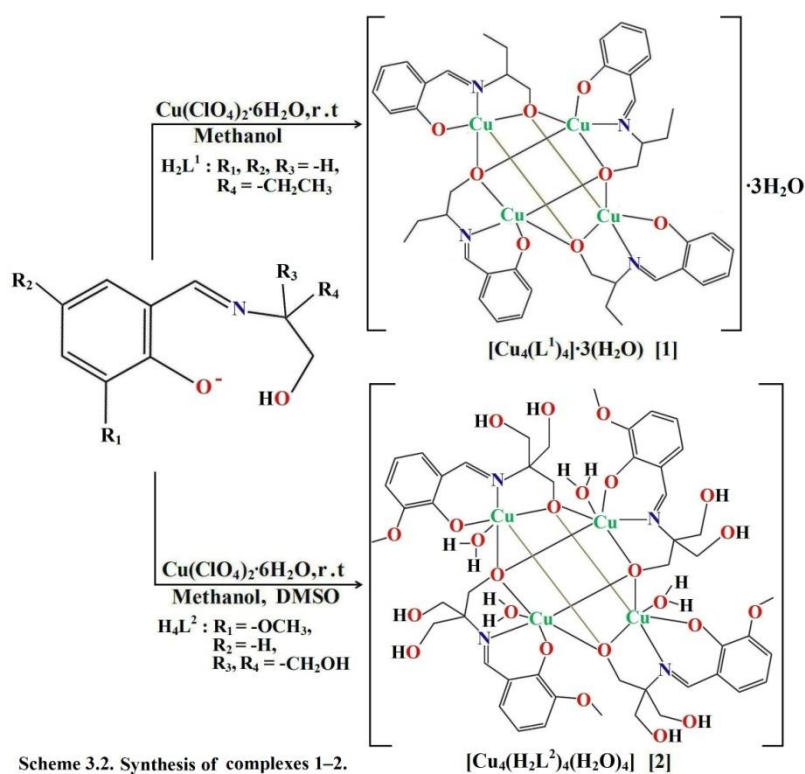
## Magnetic measurements

Temperature-dependent molar susceptibility of polycrystalline compounds were measured in a Quantum Design SQUID MPMSXL susceptometer with an applied field of 3000 and 198 G in the temperature ranges 2–300 and 2–30 K, respectively at the *Servei de Magnetoquímica* of the *Centres Científics i Tecnològics* at the Universitat de Barcelona.

### 3.2.2. Synthesis

**Caution!** Perchlorate salts of metal with organic ligands are potentially explosive and only a small amount of metal salts should be handled with care.

The complexes **1** and **2** have been synthesized adopting procedures which are schematically given in Scheme 3.2.



#### 3.2.2.1. Synthesis of ligands

##### (E)-2-((1-hydroxybutan-2-ylimino)methyl)phenol (H<sub>2</sub>L<sup>1</sup>)

A mixture of methanolic solution (20 mL) of 2-amino-1-butanol (1 mmol, 0.089 g) and salicylaldehyde (1 mmol, 0.122 g) was refluxed for 3 h. The resulting yellow colour solution was cooled to room temperature and a solid yellow compound was obtained after solvent evaporation. The compound obtained was redissolved in MeOH and filtered. The filtrate was left for slow evaporation at room temperature and yellow crystals of  $H_2L^1$  were obtained after one week. Yield: 68 %. Anal. Calc. For  $C_{11}H_{15}NO_2$  (193.24): C, 68.36; H, 7.82; N, 7.24 %. Found: C, 68.34; H, 7.79; N, 7.26 %.  $^1H$ NMR (400 MHz,  $CDCl_3$ ,  $\delta$  ppm): 0.709 - 0.886 (3H, m), 1.474-1.655 (2H, m), 2.576 (1H, s), 3.466 - 3.690 (1H, m; 2H, m), 4.957 (1H, s), 6.823 - 6.921 (1H, d; 2H, m), 7.226 - 7.298 (1H, d; 2H, m), 8.306 (1H, s).  $^{13}C$  NMR ( $CDCl_3$ , 400 MHz,  $\delta$  ppm): 165.41 (Ar-C-OH), 161.71 (-CH=N-), 132.45-113.71 (Ar-C), 73.03 (-CH<sub>2</sub>-OH), 66.23 (=N-CH-), 25.05 (-CH<sub>2</sub>-), 10.51 (-CH<sub>3</sub>).

**2-((2-hydroxy-3-methoxybenzylidene)amino)-2-hydroxymethylpropane-1,3-diol ( $H_4L^2$ )**

A methanolic solution (10 mL) of tris(hydroxymethyl)amino methane (1 mmol, 0.121 g) was added dropwise to a methanolic solution (10 mL) of 3-methoxysalicylaldehyde (1 mmol, 0.152 g) with constant stirring. Resulting yellow reaction mixture was stirred for 2 h and a yellow colour compound was separated out and filtered. The crude product was re-dissolved in methanol and filtered; the filtrate was allowed to evaporate in a refrigerator. Yellow crystalline compound was obtained from the filtrate after a few days. Yield: 70 %. Anal. Calc. for  $C_{12}H_{17}NO_5$  (255.27): C, 56.46; H, 6.71; N, 5.49 %. Found: C, 56.44; H, 6.70; N, 5.51 %.  $^1H$  NMR (DMSO- $d_6$ , 400 MHz,  $\delta$ , ppm): 4.907 (s, 1H, phenolic-OH), 8.456 (s, 1H, imine), 6.944, 6.924 (doublet, 1H, Ar), 6.890, 6.871 (doublet, 1H, Ar), 6.581, 6.563, 6.542 (m, 1H, Ar), 3.611 (s, 6H, CH<sub>2</sub>), 3.718 (s, 3H, OMe), 3.525 (s, 2H, H<sub>2</sub>O).  $^{13}C$  NMR (DMSO- $d_6$ , 400 MHz,  $\delta$ , ppm): 164.266 (-CH=N-), 159 (Ar-C-OMe), 149.754 (Ar-C-OH), 124.343 (Ar-C-imine), 114.551-117.174 (Ar-C), 66.520 (-CH<sub>2</sub>-OH), 61.311 (tertiary carbon), 55.881 (-OCH<sub>3</sub>).

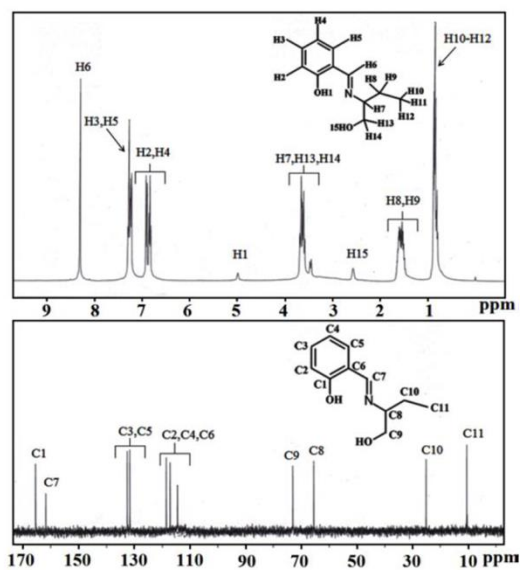


Figure 3.1.  $^1\text{H}$  and  $^{13}\text{C}$  NMR spectrum of  $\text{H}_2\text{L}^1$  recorded in  $\text{CDCl}_3$ .

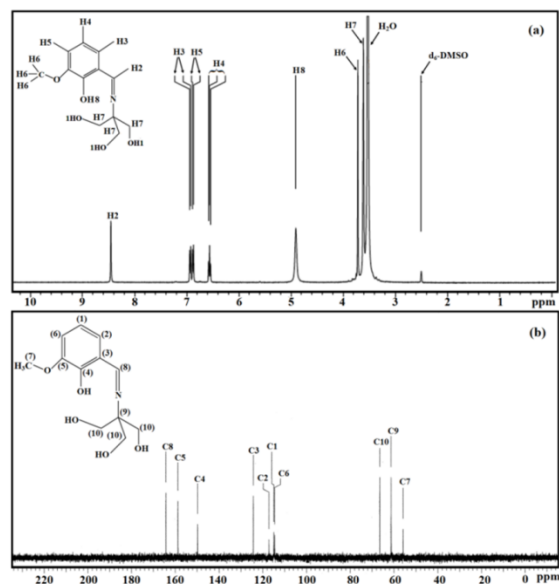


Figure 3.2.  $^1\text{H}$  (a) and  $^{13}\text{C}$  (b) NMR spectra of  $\text{H}_4\text{L}^2$  recorded in  $d_6$ -DMSO.

### 3.2.2.2. Synthesis of complexes 1 and 2

#### $[\text{Cu}_4(\text{L}^1)_4] \cdot 3(\text{H}_2\text{O})$ (1)

To a methanolic solution (10 mL) of  $\text{H}_2\text{L}^1$  (1 mmol, 0.193 g) a methanolic solution (5 mL) of triethylamine (2 mmol, 0.202 g) was added dropwise with constant stirring. To this resulting solution, dropwise addition of methanolic solution (10 mL) of  $\text{Cu}(\text{ClO}_4)_2 \cdot 6\text{H}_2\text{O}$  (1 mmol, 0.370 g) changes solution colour in deep green. The total reaction mixture was stirred for 2

hours at room temperature and filtered. The filtrate was kept in air for slow evaporation at room temperature. Green single crystals suitable for X-ray diffraction were obtained after a few days. Yield: 78 %. Anal. Calc. for  $C_{44}H_{58}Cu_4N_4O_{11}$  (1073.10): C, 49.24; H, 5.44; N, 5.22%. Found: C, 49.22; H, 5.45; N, 5.21.

### **[Cu<sub>4</sub>(H<sub>2</sub>L<sup>2</sup>)<sub>4</sub>(H<sub>2</sub>O)<sub>4</sub>] (2)**

This complex was synthesized following the procedure adopted for complex **1** using H<sub>4</sub>L<sup>2</sup> (1 mmol, 0.255 g) instead of H<sub>2</sub>L<sup>1</sup>. After one week, green compound was separated out and the compound was re-dissolved in DMSO and filtered. Green crystals suitable for X-ray analysis were obtained after two weeks. Yield: 72 %. Anal. Calc. for  $C_{48}H_{68}Cu_4N_4O_{24}$  (1339.25): C, 43.05; H, 5.12; N, 4.18%. Found: C, 43.09; H, 5.07; N, 4.06.

### **3.2.3. Crystallographic Data Collection and Refinement**

Intensities data for crystal structure analyses of compounds **1–2** were collected at room temperature on a Bruker Smart Apex diffractometer equipped with CCD with Mo-K $\alpha$  radiation ( $\lambda = 0.71073 \text{ \AA}$ ). Cell refinement, indexing, and scaling of the data sets were performed using the program Bruker Smart Apex, and Bruker Saint packages.<sup>[3.14a]</sup> Both structures were solved by direct methods and subsequent Fourier analyses<sup>[3.14b]</sup> and refined by the full-matrix least-squares method based on  $F^2$  with all observed reflections.<sup>[3.14b]</sup> The difference Fourier map of **1** revealed the presence of two residuals interpreted as water oxygens (half occupancy, H atoms not assigned) that count for three molecules for Cu<sub>4</sub>O<sub>4</sub> unit. Graphics were drawn with programs Cameron<sup>[3.14c]</sup> and Diamond 3.1.<sup>[3.14d]</sup> Crystal data and details of structure refinements are given in Table 3.1.

**Table 3.1. Crystal data and details of structure refinement for compounds 1 and 2.**

	1	2
Empirical formula	C <sub>44</sub> H <sub>58</sub> Cu <sub>4</sub> N <sub>4</sub> O <sub>11</sub>	C <sub>48</sub> H <sub>68</sub> Cu <sub>4</sub> N <sub>4</sub> O <sub>24</sub>
Formula mass, g mol <sup>-1</sup>	1073.10	1371.16
Crystal system	Tetragonal	Tetragonal
Space group	<i>I</i> 4 <sub>1</sub> /a	<i>I</i> 4 <sub>1</sub> /a
<i>a</i> , Å	15.885(3)	18.8242(5)
<i>c</i> , Å	18.894(4)	15.4961(5)
<i>V</i> , Å <sup>3</sup>	4767.8(18)	5491.1(3)
<i>Z</i>	4	4
<i>D</i> <sub>(calc)</sub> , g cm <sup>-3</sup>	1.495	1.620
$\mu$ (Mo-K $\alpha$ ), mm <sup>-1</sup>	1.820	1.615
<i>F</i> (000)	2216	2768
Theta range, deg	2.82 - 25.51	3.41 - 26.19
No. of colld data	28990	6391
No. of unique data	2212	2754
<i>R</i> <sub>int</sub>	0.0690	0.0305
Obs reflections [ <i>I</i> > 2 $\sigma$ ( <i>I</i> )]	1358	2097
Goodness of fit ( <i>F</i> <sup>2</sup> )	1.073	1.072
Parameters refined	160	186
<i>R</i> 1 [ <i>I</i> > 2 $\sigma$ ( <i>I</i> )] <sup>a</sup>	0.0401	0.0715
<i>wR</i> 2 [ <i>I</i> > 2 $\sigma$ ( <i>I</i> )] <sup>a</sup>	0.0896	0.1901
Residuals, e Å <sup>-3</sup>	0.346, -0.311	1.320, -0.598

$$^a R1(F_o) = \sum ||F_o| - |F_c|| / \sum |F_o|, wR2(F_o^2) = [\sum w(F_o^2 - F_c^2)^2 / \sum w(F_o^2)^2]^{1/2}$$

### 3.3. Results and discussion

#### 3.3.1. Molecular structure of complexes [Cu<sub>4</sub>(L<sup>1</sup>)<sub>4</sub>]·3(H<sub>2</sub>O) (1) and [Cu<sub>4</sub>(H<sub>2</sub>L<sup>2</sup>)<sub>4</sub>(H<sub>2</sub>O)<sub>4</sub>] (2)

A perspective view of the molecular structure of complexes [Cu<sub>4</sub>(L<sup>1</sup>)<sub>4</sub>] and [Cu<sub>4</sub>(H<sub>2</sub>L<sup>2</sup>)<sub>4</sub>(H<sub>2</sub>O)<sub>4</sub>] is depicted in Figures 3.3 and 3.4, respectively, and relevant bond distances and angles are summarized in Table 3.2. Both the complexes consist of neutral tetrameric moiety comprising four Cu(II) ions and four symmetry related di-anionic Schiff base ligands to form a cubane-like core of alternating copper and oxygen atoms that occupy the corners of the cube.

**Table 3.2. Bond lengths (Å) and angles (°)  
for complexes 1 and 2**

	1	2
Cu-O(1)	1.894(3)	1.915(4)
Cu-O(2)	1.975(3)	1.947(4)
Cu-N(1)	1.926(4)	1.956(5)
Cu-O(2)'	1.994(3)	1.970(4)
Cu-O(2)''	2.349(3)	2.569(4)
Cu-O(6)	-	2.797(6)
O(1)-Cu-N(1)	92.92(16)	94.0(2)
O(1)-Cu-O(2)	177.12(12)	172.15(18)
O(2)-Cu-N(1)	84.22(16)	84.6(2)
O(1)-Cu-O(2)'	96.10(12)	94.68(17)
N(1)-Cu-O(2)'	155.62(14)	166.3(2)
O(2)-Cu-O(2)'	86.41(12)	88.21(18)
O(1)-Cu-O(2)''	104.50(12)	94.16(16)
N(1)-Cu-O(2)''	121.05(13)	117.4(2)
O(2)-Cu-O(2)''	77.35(11)	79.74(16)
O(2)'-Cu-O(2)''	78.39(11)	72.49(16)

Symmetry codes: for 1 (')  $-y+5/4, x-3/4, -z+1/4$ , (")  $y+3/4, -x+5/4, -z+1/4$ ; for 2 (')  $-y+5/4, x+1/4, -z+1/4$ , (")  $-x+1, -y+3/2, z$ .

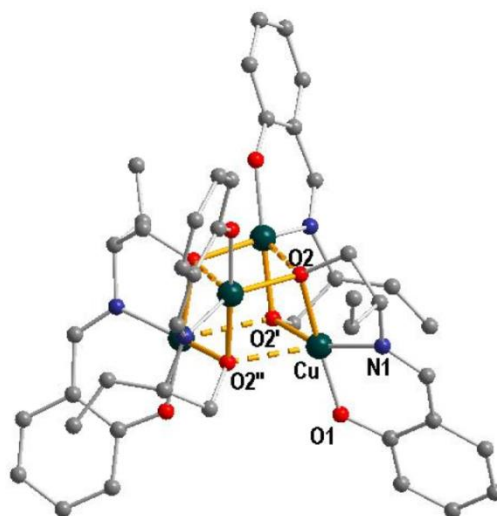


**Figure 3.3. Molecular structure of complex 1 (dotted lines indicate long Cu-O bond distances).**

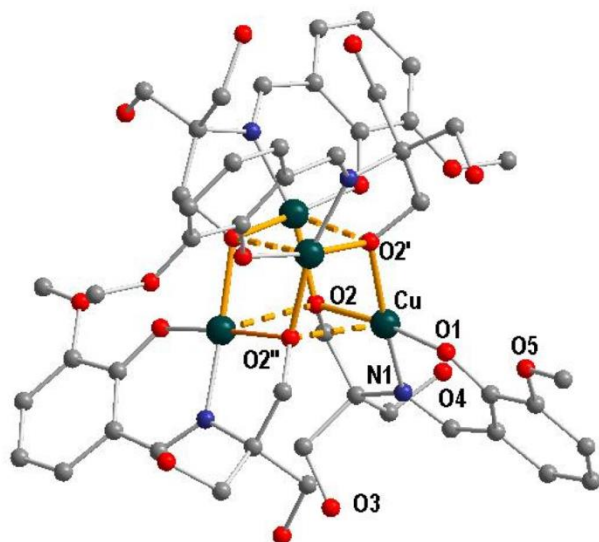


Figure 3.4. Molecular structure of complex **2** (dotted lines indicate long Cu-O bond distances). The water molecule bound at each copper ion (Cu-O<sub>w</sub>=2.797(6) Å) not shown for sake of clarity.

In fact each copper center is chelated by the tridentate Schiff base ligand through the imine nitrogen, the phenoxo and the deprotonated alkoxy oxygen atoms, and in addition is bound to two deprotonated alkoxy O atoms from symmetry related ligands. With these donor atoms copper ions in complex **1** exhibit a square pyramidal geometry, while a highly distorted hexagonal environment is detected in **2** for the presence of an additional aqua ligand located at longer distance. The Addison index ( $\tau$ )<sup>[3,15]</sup> to define the distortion of the coordination environment from trigonal bipyramidal (TBP) to square pyramidal (SP) is calculated to be 0.358 in **1**. In both complexes the doubly deprotonated ligands are found in  $\eta^3:\eta^1:\eta^1:\mu_3$  coordination mode. In complex **1** the basal distances Cu-O and Cu-N range from 1.894(3) to 1.994(3) Å, while the fifth site at apical position filled by a deprotonated alkoxy O atom shows a longer contact of 2.349(3) Å. Correspondently the equatorial distances in **2** fall in a narrower range (1.915(4)-1.970(4) Å), while the axial oxygen donors, of an alkoxy oxygen and water molecule, are at 2.569(4) and 2.797(6) Å, respectively, the latter indicating a very weak interaction. In the ligand H<sub>2</sub>L<sup>2</sup> the methoxy group on the ring does not participate in coordination as well as the two CH<sub>2</sub>-OH fragments that are far apart from the Cu<sub>4</sub>O<sub>4</sub> core. An interesting feature of complex **1** compared to **2** is the shorter Cu-O distance at apical position

(2.349(3) vs 2.569(4) Å) and the different stereochemistry of ligand disposition about the metals as discussed below.

Alvarez *et al.*<sup>[3,16]</sup> in order to study the magneto structural correlations, used the Cu···Cu distances within the Cu<sub>4</sub>O<sub>4</sub> cubane unit to classify these complexes: (i) 2+4, comprising two short and four long Cu···Cu distances, (ii) 4+2, with four short and two long Cu···Cu distances, and (iii) 6+0, which contains six similar Cu···Cu distances. The present complexes having a S<sub>4</sub> symmetry are of type (ii) with Cu···Cu short and long distances of 3.097 and 3.372 Å in **1** and of 3.190, 3.479 Å in **2**, respectively.

Since the lattice water molecules are disordered in the crystal of complex **1** (occupancy of 0.25 and 0.5) we interpret the complexes as isolated species in the crystal. On the contrary the water molecule in **2** forms H-bond connections with phenolato O1 and hydroxyl oxygen O4 (Table 3.3) of symmetry related complexes giving rise to a 3D network. The long Cu-O6 (water) bond distance of 2.797(6) Å observed in **2** is likely modulated with the aim for the water molecule to realize the cited H-bonds.

Table 3.3. H-bond parameters in complex 2.

D-H	d(D-H)	d(H..A)	<DHA	d(D..A)	A	Symmetry code A
O(4)-H(4a)	0.82	2.13	159	2.910(11)	O(6)	-
O(6)-H(16)	0.85	1.93	154	2.713(10)	O(4)	-1/4+y,3/4-x,-1/4+z
O(6)-H(26)	0.85	1.99	165	2.821(7)	O(1)	-1/4+y,5/4-x,1/4-z

However, it is worth of note that the two complexes here reported have a different stereochemistry as shown in the schematic illustrations of Figures 3.5 and 3.6, where the ligands have been simplified, thus removing ethyl substituents in **1** and methoxy and CH<sub>2</sub>OH groups in **2**. The difference is clearly evident, especially by comparison of Figures 3.5b and 3.6b, showing the arrangement of ligands about the tetranuclear Cu<sub>4</sub> core.

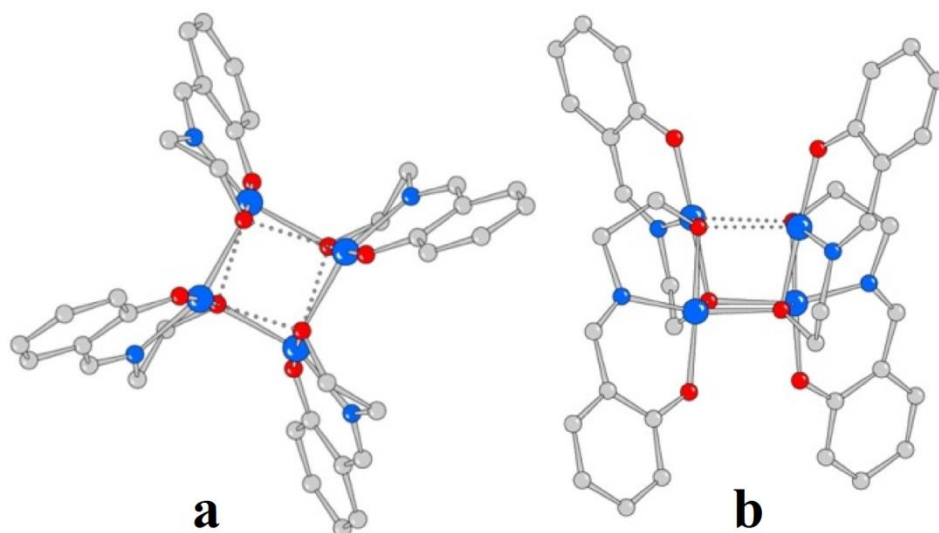


Figure 3.5. Complex 1 viewed down the  $S_4$  symmetry axis and a perspective side view (H-atoms and ethyl groups not shown).

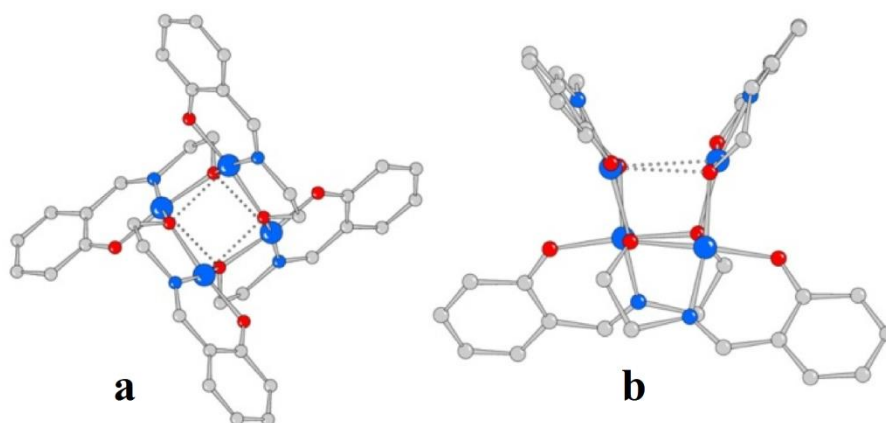


Figure 3.6. Complex 2 viewed down the  $S_4$  symmetry axis and a perspective side view (H-atoms, methoxy and  $\text{CH}_2\text{OH}$  groups removed for clarity). The ligands arrangement is similar to that detected in all the complexes structurally characterized and reported to date.

The Cambridge structural database<sup>[3.17]</sup> was searched for similar complexes comprising a tetranuclear  $\text{Cu}_4\text{O}_4$  core built by variously substituted salicylidene-ethanolato ligands of Scheme 3.2. The structures retrieved (beside the recently published structures of Colacio *et al.*)<sup>[3.18]</sup> are summarized in Table 3.4, where the Cu-O distances and space groups are also reported. Some of the complexes, built with the same ligands,<sup>[3.15–3.17,3.19–3.20,3.21–3.22,3.26–3.27,3.31–3.32]</sup> crystallize in different space groups tuned in some cases by the presence of lattice solvent molecules, which affect the packing.

**Table 3.4. Structural and the exchange coupling constants data of complexes [CuL]<sub>4</sub> (L=tridentate salicylidene-ethanolato ligands).**

Complex	Space group	Class	$\alpha(\text{Cu-O-Cu})$ /°	Cu-O/N short distances (Å)	Cu-O long distances (Å)	$d_2(\text{Cu}\cdots\text{Cu})$ [Å]	$J_{\text{exp}}$ [cm <sup>-1</sup> ]	ref
[Cu <sub>4</sub> (L <sup>1</sup> ) <sub>4</sub> ].3(H <sub>2</sub> O)	<i>I</i> 4 <sub>1</sub> /a	4+2	102.6	1.894(3)- 1.994(3)	2.349(3)	3.097-3.372	Antiferromagnetic, $J_1 = -20.3 \text{ cm}^{-1}$ , $J_2 = 0 \text{ cm}^{-1}$	This work
[Cu <sub>4</sub> (L <sup>2</sup> ) <sub>4</sub> (H <sub>2</sub> O) <sub>4</sub> ]	<i>I</i> 4 <sub>1</sub> /a	4+2	88.3	1.915(4)- 1.970(4)	2.569(4)	3.191-3.480	Ferromagnetic, $J_1 = 101.1 \text{ cm}^{-1}$ , $J_2 = -51.5 \text{ cm}^{-1}$	This work
[{Cu(H <sub>2</sub> L <sup>3</sup> ) <sub>4</sub> }]	<i>P</i> 2 <sub>1</sub> /c	4+2	88.45–107.97	1.868(4)- 1.968(4)	2.401(4)- 2.506(4)	3.114–3.378	Ferromagnetic, +28.7, +7.8	3.18
[{Cu(H <sub>2</sub> L <sup>4</sup> ) <sub>4</sub> }]	<i>P</i> $\bar{1}$	4+2	89.95–109.50	1.890(1)- 1.999(2)	2.282(1)- 2.600(1)	3.058–3.384	Ferromagnetic, +39.8, +10.2	3.18
[Cu <sub>4</sub> (H <sub>2</sub> L <sup>5</sup> ) <sub>4</sub> ]	<i>I</i> 4 <sub>1</sub> /a	-	-	1.906(2)- 1.945(2)	2.5930(16)	-	-	3.19
[Cu <sub>8</sub> (L <sup>3</sup> ) <sub>8</sub> ].2EtOAc. H <sub>2</sub> O	<i>P</i> 2 <sub>1</sub> /c	-	-	1.952-1.984	2.433-2.531	-	-	3.20
[Cu <sub>4</sub> (L <sup>6</sup> ) <sub>2</sub> (HL <sup>6</sup> ) <sub>2</sub> (H <sub>2</sub> O)](ClO <sub>4</sub> ) <sub>2</sub> .2H <sub>2</sub> O	<i>P</i> 2 <sub>1</sub> /n	4+2	106.1-119.8	1.956 - 2.001	2.467 - 2.561	3.351-3.752	Antiferromagnetic, $J_{\text{av}} = -99.0$ .	3.21
[Cu <sub>4</sub> (NSI) <sub>4</sub> ]. 2C <sub>2</sub> H <sub>5</sub> OH.2H <sub>2</sub> O	<i>P</i> 2 <sub>1</sub>	4+2	108.7-110.9	1.927 - 1.972	2.541 - 2.644	3.176–3.531	Ferromagnetic, $J = 5.15$	3.22
[Cu <sub>4</sub> (L <sup>7</sup> ) <sub>4</sub> ].5CH <sub>3</sub> OH. H <sub>2</sub> O	<i>P</i> $\bar{1}$	4+2	102.0-109.4	1.931 - 1.984	2.373 - 2.580	3.095-3.413	Ferromagnetic, $J_1 = -15.8(6)$ , $J_2 = 33(1)$	3.23
[Cu <sub>4</sub> (HL <sup>8</sup> ) <sub>4</sub> ]	<i>P</i> 2 <sub>1</sub> /c	-	-	1.895(3)- 1.960(3)	2.515(3)- 2.772(3)	-	-	3.24
[Cu <sub>3</sub> Mn(L <sup>9</sup> ) <sub>4</sub> (H <sub>2</sub> O) <sub>2</sub> ]. (PF <sub>6</sub> ) <sub>2</sub> .2(Et <sub>2</sub> O)	<i>P</i> 2/c	-	-	1.952 - 1.957	2.512 - 2.533	-	-	3.25
[Cu <sub>4</sub> (L <sup>10</sup> ) <sub>4</sub> ]	<i>P</i> 2 <sub>1</sub> /c	-	-	1.892(2)- 1.972(2)	2.381(2)- 2.473(2)	-	-	3.26
[Cu <sub>4</sub> (H <sub>2</sub> L <sup>5</sup> ) <sub>4</sub> ]	<i>P</i> $\bar{1}$	-	-	1.8982(13)- 1.9563(13)	2.467(1)- 2.565(1)	-	-	3.26
[Cu <sub>4</sub> L <sup>11</sup> ].2H <sub>2</sub> O	<i>P</i> bcn	4+2	101.3-106.1	1.951 - 1.973	2.439 - 2.455	3.06-3.48	Ferromagnetic, $J_1 = +64.8$ , $J_2 =$ $+24.4$ and $J_3 = +3.0$	3.27
[Cu <sub>4</sub> (hsae) <sub>4</sub> ].2H <sub>2</sub> O. 4CH <sub>3</sub> CN	<i>C</i> 2/c	4+2	104.8-106.1	1.930 - 1.960	2.467 - 2.561	3.108-3.615	Ferromagnetic, $J_1 = -17.6(1)$ , $J_2 = +36.0(9)$	3.28
[Cu <sub>4</sub> (HL <sup>12</sup> ) <sub>2</sub> (L <sup>12</sup> ) <sub>2</sub> (Me OH) <sub>2</sub> ](ClO <sub>4</sub> ) <sub>2</sub> .(MeOH ) <sub>2</sub> . (H <sub>2</sub> O)	<i>P</i> 2 <sub>1</sub>	-	-	1.927 - 1.991	2.442 - 2.985	-	-	3.29
[Cu <sub>4</sub> (L <sup>13</sup> ) <sub>4</sub> ].(CH <sub>3</sub> CN) <sub>2</sub>	<i>P</i> 2 <sub>1</sub>	-	-	1.926 - 1.956	2.423 – 2.841	-	-	3.30
l-[Cu <sub>4</sub> (HL <sup>12</sup> ) <sub>2</sub> (L <sup>12</sup> ) <sub>2</sub> (MeOH) <sub>2</sub> ](NO <sub>3</sub> ) <sub>2</sub> . MeOH	<i>P</i> 2 <sub>1</sub>	4+2	90.24-127.66	1.933 - 1.991	2.448 - 3.239	3.1522(9) - 4.0593(9)	Antiferromagnetic, $J_{\text{M}} = J_{\text{T}} = -149(3)$ , $J^{\text{S}} = -18(5)$ .	3.31
SOPAK	<i>P</i> 4 <sub>2</sub> /n	-	-	1.953 - 1.965	2.421	-	-	3.32
[Cu <sub>4</sub> (L <sup>14</sup> ) <sub>4</sub> ]	<i>I</i> 4 <sub>1</sub> /a	-	-	1.950 - 1.964	2.439	-	-	3.33
[Cu <sub>4</sub> (H <sub>2</sub> L <sup>15</sup> ) <sub>4</sub> ].10H <sub>2</sub> O	<i>I</i> 4 <sub>1</sub> /a	4+2	89.45- 106.71	1.962 - 1.967	2.482	-	ferromagnetic, $2J_1 = -33.5(2)$ , $2J_2 = 67.0(3)$ .	3.34
[{Cu(sae) <sub>4</sub> }. 2CH <sub>3</sub> OH.H <sub>2</sub> O}]	<i>P</i> 2 <sub>1</sub> /c	-	-	1.952 – 1.973	2.396 - 2.515	-	-	3.35
[Cu <sub>4</sub> (HL <sup>16</sup> ) <sub>4</sub> ]	<i>C</i> 2/c	4+2	1.90-1.92	1.882(5)- 1.928(6)	3.48, 3.199	3.40–3.45	Antiferromagnetic, $J = -74.7$	3.36
[Cu <sub>4</sub> (HL <sup>16</sup> ) <sub>4</sub> ]. 3.5 MeOH.2.25 H <sub>2</sub> O	<i>P</i> 2 <sub>1</sub> /c	4+2	86.6-116.0	1.873(6)- 1.978(6)	2.481-2.739	3.116–3.533	Antiferromagnetic, $J_1 = -3.2$ , $J_2 = +1.1$	3.36

$H_2L^3$ , *N*-(2-hydroxyethyl)-3,5-di-*tert*-butylsalicylaldimine;  $H_2L^4$ , *N*-(2-hydroxyethyl)-4-methoxysalicylaldimine;  
 $H_4L^5$ , 2-[(2-Hydroxybenzylidene)-amino]-2-hydroxymethyl-propane-1,3-diol;  
 $H_2L^6$ , 2-[(2-hydroxy-ethylimino)-methyl]-6-methoxy-phenol; NSI, hydroxyethylsalicydenimine;  
 $H_2L^7$ , 2-(5-fluorosalicylideneamino)ethanol;  $H_3L^8$ , 2-[(2-Hydroxybenzylidene)-amino]-2-methyl-propane-1,3-diol;  
 $H_2L^9$ , 4-Bromo-2-[(2-hydroxyethylimino)methyl]phenol;  $H_2L^{10}$ , 2-[(2-Hydroxyethylimino)methyl]phenol;  
 $H_2L^{11}$ , 4-chloro-2-[(*E*)-(2-hydroxyethylimino)methyl]phenol;  $H_2hase$ , (2-(4-hydroxysalicylideneamino)ethanol);  
 $H_2L^{12}$ , 2-[(1-Benzyl-2-hydroxyethylimino)methyl]-6-methoxyphenol;  $H_2L^{13}$ , 1-[(1-Hydroxymethylpropylimino)methyl]  
naphthalene-2-ol;  $H_2L^{14}$ , 1-[(2-Hydroxyethylimino)methyl]naphthalene-2-ol;  $H_2L^{15}$ , tris(hydroxymethyl)(2-hydroxybenzylamino)  
methane; *sae*, 2-salicylideneamino-1-ethanol;  $H_2L^{16}$ , 2-( $\beta$ -naphthalideneamino)-2(hydroxymethyl)-1-propanol.

Although in the majority of cases the complexes do not reside about an improper fourfold axis, the symmetry is close to a pseudo- $S_4$ , being the differences in solid state imposed by the packing or the different conformation of substituents on the ligands. Some observations are worth of note from Table 3.4: the coordination bond lengths fall in the range 1.882-2.001 Å, that is within 2-3 e.s.d's. in most cases. On the other hand a large range is detected for the long  $Cu \cdots O$  distances. In particular values up to 3.0 Å were measured associated with a boat conformation of the  $Cu_4O_4$  central moiety,<sup>[3.23-3.24,3.31]</sup> dictated by the existence of  $\pi$ - $\pi$  interactions between the naphthyl rings. Actually it is worth of note that all the cubane like structures reported so far present the same arrangement of ligands, namely as that schematically depicted for complex **2** (Figure 3.6).

Thus at our knowledge complex **1** represents the first example where the tridentate Schiff bases assume a different configuration about the tetranuclear  $Cu_4O_4$  core, as described above. An inspection of Table 3.2 indicates that in complex **1** the four symmetry related  $Cu \cdots O$  distances of 2.349(3) Å are the shortest among those reported, likely indicating that this configuration lead to a more compacted  $Cu_4O_4$  moiety.

### 3.3.2. Electronic absorption spectra of ligands

The electronic spectra of  $H_2L^1$  and  $H_4L^2$  were recorded in methanol (Figure 3.7). The electronic absorption spectrum of  $H_2L^1$  exhibits three sharp bands at 216 nm ( $\epsilon \sim 6.33 \times 10^4$

liter mole<sup>-1</sup> cm<sup>-1</sup>), 253 nm ( $\epsilon \sim 3.43 \times 10^4$  liter mole<sup>-1</sup> cm<sup>-1</sup>), 280 nm ( $\epsilon \sim 4.02 \times 10^3$  liter mole<sup>-1</sup> cm<sup>-1</sup>) and 316 nm ( $\epsilon \sim 9.44 \times 10^3$  liter mole<sup>-1</sup> cm<sup>-1</sup>). The spectrum of H<sub>4</sub>L<sup>2</sup> shows significant transitions at 202 nm ( $\epsilon \sim 8.82 \times 10^4$  liter mole<sup>-1</sup> cm<sup>-1</sup>), 241 nm ( $\epsilon \sim 7.97 \times 10^4$  liter mole<sup>-1</sup> cm<sup>-1</sup>), 293 nm ( $\epsilon \sim 5.80 \times 10^4$  liter mole<sup>-1</sup> cm<sup>-1</sup>) and 420 nm ( $\epsilon \sim 2.51 \times 10^4$  liter mole<sup>-1</sup> cm<sup>-1</sup>).

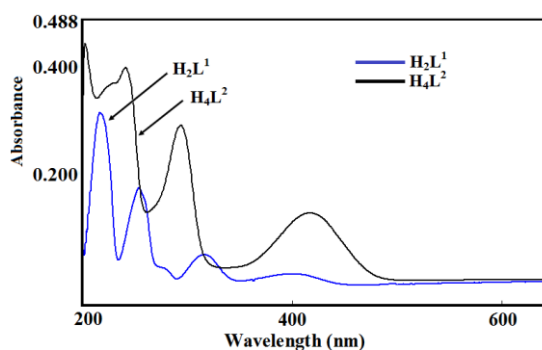


Figure 3.7. Electronic spectra of ligand H<sub>2</sub>L<sup>1</sup> (blue) and H<sub>4</sub>L<sup>2</sup> (black).

### 3.3.3. FTIR, Electronic absorption and fluorescence spectra of complexes 1 and 2

The IR spectra of complexes **1** and **2** are shown in Figure 3.8, and the most of the significant absorption bands are summarized in the experimental section. The spectrum of complex **2** exhibits a strong broad band in the region 3200-3600 cm<sup>-1</sup>, due to the  $\nu(\text{O-H})$  stretching vibration of free hydroxyl group of ligand. The bands at 2985 cm<sup>-1</sup> for complex **1** and 2982 cm<sup>-1</sup> for complex **2** correspond to the aromatic  $\nu(\text{C-H})$  stretching vibrations while aliphatic  $\nu(\text{C-H})$  stretching vibrations for complexes **1** and **2** appear at 2943 and 2946 cm<sup>-1</sup> respectively. On the other hand for complex **2** the band at 1218 cm<sup>-1</sup> corresponds to  $\nu(\text{O-CH}_3)$  stretching vibrations.

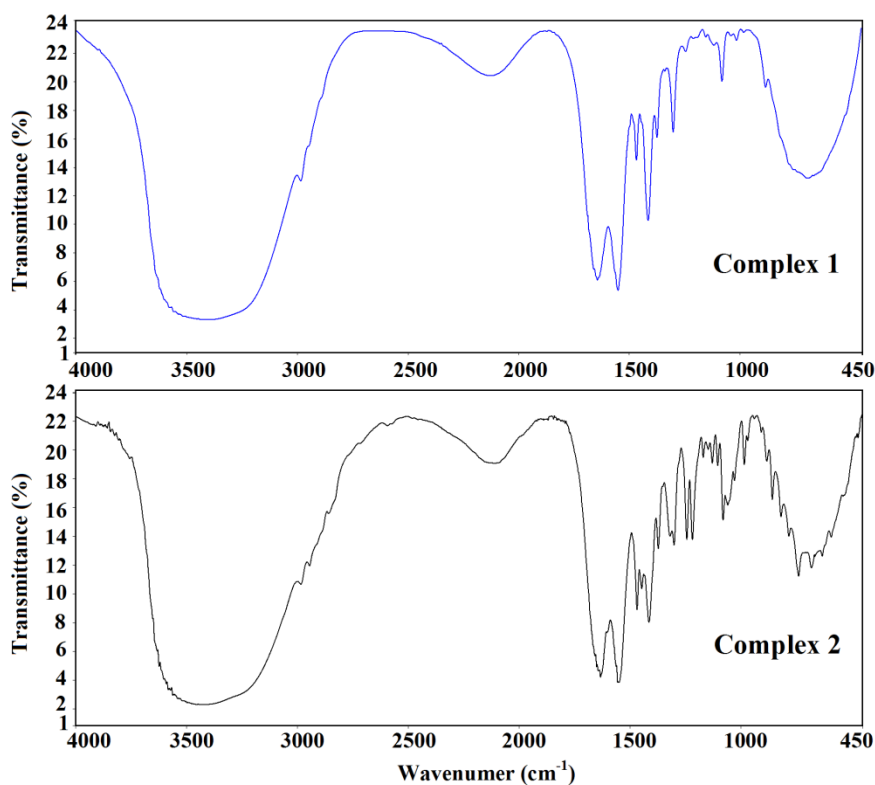


Figure 3.8. IR spectrum of complex 1 (blue) and 2 (black).

The absorption and emission spectra of complexes **1** and **2** were recorded in methanol at room temperature. The electronic absorption spectrum of **1** shows transition at 239 nm ( $\epsilon \sim 8.99 \times 10^5 \text{ L mole}^{-1} \text{ cm}^{-1}$ ), 268 nm ( $\epsilon \sim 5.69 \times 10^5 \text{ L mole}^{-1} \text{ cm}^{-1}$ ) and 365 nm ( $\epsilon \sim 2.57 \times 10^5 \text{ L mole}^{-1} \text{ cm}^{-1}$ ). On excitation at 365 nm, **1** exhibits luminescence bands at 419 nm (Figure 3.9). On the other hand the electronic absorption spectrum of complex **2** shows transition at 209 nm ( $\epsilon \sim 9.55 \times 10^5 \text{ L mole}^{-1} \text{ cm}^{-1}$ ) and 229 nm ( $\epsilon \sim 3.48 \times 10^5 \text{ L mole}^{-1} \text{ cm}^{-1}$ ) and exhibits luminescence bands at 309, 332, and 342 nm on excitation at 229 nm (Figure 3.10).

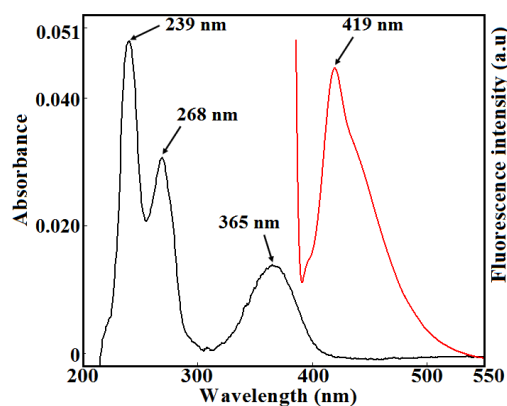


Figure 3.9. Absorption (left) and fluorescence (right) spectra of complex 1.

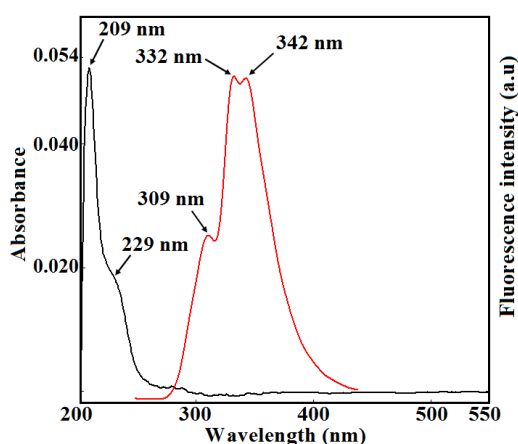
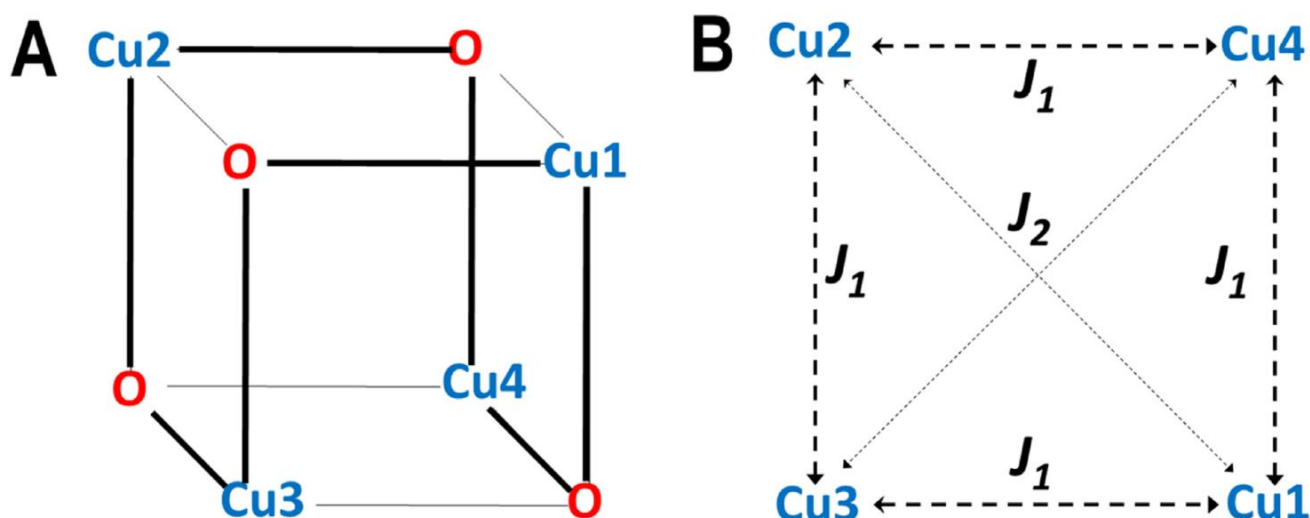


Figure 3.10. Absorption (left) and fluorescence (right) spectra of complex 2.

### 3.3.4. Magnetic properties of complexes

The  $\chi_M T$  versus  $T$  curve for complex **1** starts from a value of  $1.47 \text{ cm}^3 \text{ K mol}^{-1}$  at room temperature, in agreement with the value of  $1.48 \text{ cm}^3 \text{ K mol}^{-1}$  expected for four uncoupled  $S=1/2$  spins assuming  $g=2$ , and decreases continuously until  $0.04 \text{ cm}^3 \text{ K mol}^{-1}$  is reached at 10 K. Below this temperature the  $\chi_M T$  value decreases smoothly, showing the tendency to form a plateau at a value different than 0. This behavior evidences the presence of an overall antiferromagnetic interaction and an  $S=0$  ground state in the complex, suggesting the presence of small amounts of paramagnetic mononuclear impurities. On the other hand the  $\chi_M T$  versus  $T$  curve for complex **2** shows a value of  $2.06 \text{ cm}^3 \text{ K mol}^{-1}$  at room temperature, which is significantly higher than the value expected for four uncoupled  $S=1/2$  spins

assuming  $g=2$ . The curve increases exponentially up to a value of  $2.67 \text{ cm}^3 \text{ K mol}^{-1}$  at 34 K. Below this temperature the  $\chi_{\text{M}}T$  versus  $T$  curve decreases sharply down to a  $\chi_{\text{M}}T$  value of  $0.85 \text{ cm}^3 \text{ K mol}^{-1}$  at 2 K. As opposed to complex **1**, relatively strong ferromagnetic exchange interactions are operating in complex **2**, despite the similar skeleton of the two compounds. Both complexes present a cubane-like structure characterized by a  $[\text{Cu}_4\text{O}_4]$  core that possesses four short and two long  $\text{Cu}\cdots\text{Cu}$  distances as a result of the particular relative arrangement of the axial axes and equatorial planes of the  $\text{Cu(II)}$  ions, leading to a [4+2] geometric type of cubane compounds proposed by Ruiz *et al.*<sup>[3.12b]</sup> The corresponding equatorial or axial character of the bridging atoms with respect to the two connected  $\text{Cu(II)}$  ions in each pair is shown in Scheme 3.3A.



Scheme 3.3. A) Structural arrangement of a [4+2] cubane structure like the one of complexes **1** and **2**, where short (equatorial) and long(axial) Cu-O bonds have been illustrated with thick and thin lines, respectively. B) Magnetic model used for the description of the structure represented in A, where  $J_1$  and  $J_2$  describe the magnetic exchange pathways through  $\text{Cu(II)}$  pairs showing short and long Cu-Cu distances, respectively.

Taking this structural arrangement in consideration, the magnetic behavior of the two complexes can be studied by employing the isotropic spin Hamiltonian of equation 3.1, based on the model showed in Scheme 3.3B.

$$H = J_1(S_1S_3 + S_1S_4 + S_2S_3 + S_2S_4) - J_2(S_1S_2 + S_3S_4) \quad \text{eq.3.1}$$

$J_1$  describes the magnetic exchange coupling between the four  $\text{Cu(II)}$  pairs with short  $\text{Cu}\cdots\text{Cu}$  distances, while  $J_2$  characterizes the magnetic exchange coupling between the

remaining two Cu(II) pairs with long intermetallic distance. Those pairs with short Cu...Cu distances are bridged by two different O atoms, of which one belongs to the equatorial plane of both the Cu(II) ions in the pair. On the contrary, Cu(II) pairs characterized by a long Cu...Cu distance always involve an axial coordination of the O bridging atom to one Cu(II) ion in any of their bridging pathways. Therefore, in the second case there is always a non-magnetic orbital involved in the exchange, and consequently the interaction is expected to be very weak. Thus, while  $J_1$  can be either ferro or antiferromagnetic in nature, it will be definitely stronger than  $J_2$  in these [4+2] type of cubane systems.

The  $\chi_M T$  versus T curves of complexes **1** and **2** were fitted with the PHI program.<sup>[3,37]</sup> One single g value was assigned for the four Cu(II) ions in each complex due to their equivalence in the crystal, i. e.  $g_1=g_2=g_3=g_4$ . For the spin Hamiltonian described in equation 3.1, a good agreement between the experimental and fitted curves was found with the following parameters:  $g=2.14$ ,  $J_1=-20.3 \text{ cm}^{-1}$  and  $J_2=0 \text{ cm}^{-1}$  for complex **1** and  $g=2.10$ ,  $J_1=101.1 \text{ cm}^{-1}$  and  $J_2=-51.5 \text{ cm}^{-1}$  for complex **2**. Temperature-independent paramagnetism (TIP) was considered equal to  $120 \times 10^{-6} \text{ cm}^3 \text{ mol}^{-1}$  for both complexes. Additionally the fit was improved when considering the presence of a 7% Cu(II) mononuclear impurity in complex **1**. The fitted curves are represented together with the experimental ones in Figure 3.11.

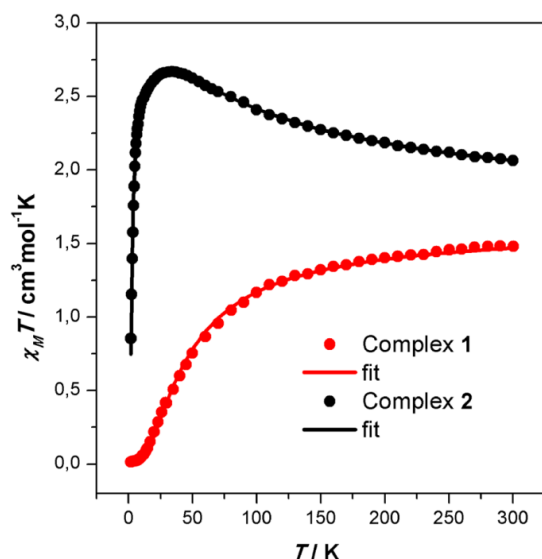


Figure 3.11. Thermal dependence of the  $\chi_M T$  for complexes 1 and 2. Points indicate experimental data and straight lines represent the best fitting curves obtained.

The nature and magnitude of  $J_i$  exchange constants in [4+2] cubane structures were theoretically studied by Tercero *et al.*<sup>[3.16]</sup> As deduced from Scheme 3.3,  $J_I$  is the result of the combined exchange through two different pathways, of which that involving two short Cu-O bonds is the most efficient, since only magnetic orbitals participate to it. According to the previously mentioned work of Tercero *et al.*, the sign and magnitude of the  $J_I$  magnetic exchange constant should correlate with the Cu-O-Cu angle characteristic of this short exchange pathway, since this will determine the degree of overlapping between the two magnetic orbitals of the Cu(II) ions in the pair. In fact, calculations suggest that antiferromagnetic interactions can be expected in  $[\text{Cu}_4\text{O}_4]$  compounds with angles larger than ca.  $103^\circ$ , in which case the overlapping of magnetic orbitals becomes effective.

In agreement with this prediction, Papadakis *et al.* recently reported an analogous compound exhibiting a weak antiferromagnetic  $J_I$  interaction associated to a Cu-O-Cu angle of  $103.5^\circ$ , similar to that detected for complex 1 in this work, which shows a Cu-O-Cu angle of  $102.6^\circ$ .<sup>[3.38]</sup>

However, many previously reported  $[\text{Cu}_4\text{O}_4]$  compounds with a [4+2] cubane-like structure (Table 3.4) show ferromagnetic  $J_I$  interactions, even though their Cu-O-Cu angle is larger

than  $103^\circ$ .<sup>[3.27,3.28,3.39]</sup> This is also the case of complex **2** reported in this work, which shows a moderate ferromagnetic exchange constant with a Cu-O-Cu angle of  $109^\circ$ . Several structural parameters, often correlated with the nature and magnitude of the magnetic exchange coupling have been compared between complexes **1** and **2**, but none of them seems to justify such different behavior by itself: Complex **2** shows a larger Cu-O-Cu angle, shorter Cu-O distances, a less perpendicular arrangement of the  $\{\text{Cu}_2\text{O}_2\}$  planes containing the magnetic metal orbitals and a smaller out-of-plane shift of the carbon atom connected to the bridging oxygen, and consequently all these factors would suggest a larger overlap of the magnetic orbitals and a more antiferromagnetic coupling.<sup>[3.16,3.40]</sup> Indeed, Tercero *et al.* already highlighted the disagreement between experimental results and theoretical predictions, being the former generally ferromagnetic while the latter predicted antiferromagnetic interactions. The authors suggested, by means of a theoretical experiment, that the chelating nature of the terminal ligands attached to the alkoxo bridge of the cubane structures might be the reason for the observed disagreement, since calculations were performed with a simpler non-chelating terminal ligand, while most of the examples found in literature included a chelating one. New calculations were carried out on two analogous structures, where the chelating terminal ligand attached to the alkoxo bridge was preserved in one, and theoretically broken in the other: the calculated magnetic exchange constant was substantially more ferromagnetic for the one with chelating nature. Considering that this terminal chelate introduces an additional exchange pathway between the two copper atoms, it seems reasonable that it can substantially affect the magnetic superexchange. In our case, both complexes **1** and **2** show a terminal ligand attached to the alkoxo bridge with a chelating nature. However the chelates are significantly different from a geometrical as well as from an electronic point of view. While the chelate shows a substituent of aliphatic nature in complex **1**, the substituent includes two alcohol groups in complex **2**. Additionally, the dihedral angle between the two

planes formed by the atoms at the chelate ring (Cu-N-C-C-O) are quite different, being 45.64° and 32.60° for complex **1** and **2**, respectively. As for structural issues, it should be emphasized that complex **1** represents the first example where the tridentate Schiff bases assume a different configuration about the tetranuclear Cu<sub>4</sub>O<sub>4</sub> core (Figure 3.5), being the configuration of complex **2** (Figure 3.6) the one always found for cubane systems previously reported in the literature. The different stereochemistry of complex **1** might also be behind the reasons for the antiferromagnetic behavior observed, compared to the ferromagnetic coupling usually encountered.

On the other hand, either negligible or antiferromagnetic values of  $J_2$  have been obtained, in agreement with similar [4+2] cubane compounds previously reported.<sup>[3.41,3.5e]</sup> Nevertheless, this parameter has been often observed to strongly correlate with the  $J_1$  value in the fitting procedure, and thus the  $J_2$  values obtained should be considered with caution.

### 3.4. Conclusions

In summary, it is reported here the syntheses, single-crystal structures and magnetic behaviors of two new tetranuclear [Cu<sub>4</sub>] copper(II) complexes (**1** and **2**) using polydentate Schiff base ligands, H<sub>2</sub>L<sup>1</sup> and H<sub>4</sub>L<sup>2</sup>, respectively. Variable temperature magnetic susceptibility measurements in the range 2–300K indicate overall antiferromagnetic exchange coupling in complex **1**, while ferromagnetic exchange coupling in complex **2**. The difference in magnetic behavior can be hardly ascribed to a specific or single structural parameter, but to a resulting different geometry derived from the combination of all of them: although both complexes show comparable closed cubane like core structures, the arrangement of the ligands around the Cu<sub>4</sub>O<sub>4</sub> core differs significantly, and this might be at the origin of such a different magnetic behavior.